PERGAMON

International Journal of Plasticity 15 (1999) 575–603

INTERNATIONAL JOURNAL OF Plasticity

Modeling temperature and strain rate history effects in OFHC Cu

Albert B. Tanner*, Robert D. McGinty, David L. McDowell

George W. Woodruff School of Mechanical Engineering, Georgia Institute of Technology, Atlanta, GA 30332-0405, USA

Received in revised form 24 July 1998

Abstract

In this paper, we report the modeling of a series of large strain deformation experiments on initially annealed OFHC Cu involving sequences of temperature, and strain rate (varying from quasi-static to dynamic). It is shown that equations-of-state with parameters determined using constant strain rate data from monotonic loading paths, although they employ instantaneous temperature and strain rate dependence, are insufficient to describe mechanical behavior. Macroscale internal state variable (ISV) viscoplasticity models, such as the Mechanical Threshold Stress (Follansbee, P.S., Kocks, U.F., 1988. A constitutive description of the deformation of copper based on the use of the mechanical threshold as an internal state variable. Acta Metall. 36, 81.) and BCJ–SNL (Bammann, D., Chiesa, M.L., Johnson, G.C., 1990a. A strain rate dependent flow surface model of plasticity. Sandia National Laboratory Report, SAND90-8227, Livermore, CA.) models, representative of a broad class of such models, are fit to the quasistatic isothermal and high strain rate (approximately adiabatic) data for compression and then predictions are compared to the experimental results for path sequence experiments. Implications for the representation of path history effects through the hardening, static and dynamic recovery functions are considered. A mesoscale polycrystal plasticity model with one and two slip system hardening variables is also examined in the context of sequence experiments.

1. Introduction

Improved experimental capabilities have resulted in a greater and more detailed quantity of information concerning material behavior. The understanding and

*Corresponding author.

0749-6419/98/$ - see front matter
PII: S0749-6419(98)00062-X

characterization of material responses has been greatly enhanced through process in both material test apparatuses, such as automatic controls, digital measurement systems and microprocessors, and the ability to detect and observe actual microstructure. These detailed, more accurate data permit improved state-of-the-art constitutive models to be developed which account for many of the observed material responses.

Constitutive models have evolved and become more complex as additional material responses are incorporated. Material behavior is included in internal state variable (ISV) constitutive models through the addition of appropriate internal variables, their evolutionary relationships and their coupling with the kinetic equation. Modern constitutive models do not incorporate all macroscopic behavior. Additional terms may be required to adequately predict restoration processes concurrent with or following straining such as dynamic softening, including both single and multiple peak dynamic recrystallization, and static thermal recovery. Such terms may be necessary to describe history effects resulting from arbitrary sequences of temperature, strain rate and deformation path.

Accounting for complex paths of deformation, temperature, and strain rate is an important requirement of constitutive laws for large strain problems such as high speed machining, impact, and various primary metal forming operations.

Constitutive models attempt to correlate simple experiments and predict more complex material behavior. The capability of a particular model is based on its predictive accuracy compared to actual measured experimental data which is obtained under the same temperature, strain rate and loading conditions. The utility of a particular model is also based on robustness: the ability to accurately provide predictions for conditions which have not been determined experimentally. The predictive accuracy of a given model is not the only important criterion for its usefulness; the effort required to determine the material parameters for the model also determines a model's utility. Parameter identification difficulty is related to the number and uniqueness of these parameters, their relationship to actual, physically observable behavior and the types and amount of experimental data available or necessary.

This paper reports on efforts to model history effects resulting from sequences of imposed temperature and strain rate at large strains. Such effects are relevant to applications such as metal forming or impact. The first section contains a description of three macroscale constitutive models used. Then a material parameter optimization process is discussed and then used to obtain an optimized parameter set using a range of constant strain rate data at various temperatures. Sequence effects are then predicted and compared to experiments. Additionally, the parameter sensitivity of each model is determined. The final section investigates the capability of a mesoscale model that incorporates orientation distribution of grains—continuum polycrystal plasticity—for describing sequence effects using one and two hardening variables at the level of each slip system. The intent is to build up the complexity of constitutive description from an equation-of-state model with no ISVs to macroscale models with one and two hardening ISVs, respectively, to a mesoscale model with one and two hardening ISVs for each slip system, along with the orientation

distribution of grains. Different functional forms for hardening behavior are employed in each of these models.

2. Constitutive models

Three constitutive models were selected to model the experimental sequence data, an equation-of-state model and two state-of-the-art ISV models. The Johnson/Cook model (Johnson and Cook, 1983; Johnson et al., 1983) is an empirical equation-of-state model designed for ease of computational implementation (Johnson, 1988). The Mechanical Threshold Stress (MTS) model (Follansbee and Kocks, 1988; Mecking and Kocks, 1981) and the Bammann, Chiesa, and Johnson (BCJ–SNL) model (Bammann et al., 1990a) were selected as macroscale ISV models possessing one and two ISVs, respectively.

The Johnson and Cook, 1983 equation-of-state model has enjoyed much success due to its simplicity and the availability of parameters for various materials of interest. The flow stress for the uniaxial case is given by

$$\sigma = (\sigma_0 + B\varepsilon^n)\left(1 + C\ln\frac{\dot{\varepsilon}}{\dot{\varepsilon}_0}\right)\left(1 - \left[\frac{T - T_r}{T_m - T_r}\right]^m\right) \tag{1}$$

The first term gives dependence on strain, the second represents instantaneous strain rate sensitivity and the last term represents the temperature-dependence of flow stress. This approach does not represent any thermal or strain rate history effects, but is simple to implement and the parameters are readily obtained from a limited number of experiments (Johnson, 1988). While this model is purely empirical, it is a widely used and successful constitutive model (cf. Meyers, 1994). It provides a basis of comparison for a history independent model with history dependent ISV constitutive models.

The addition of history dependent parameters is necessary to represent material behavior. These parameters represent the current state of the material, which includes strain rate and temperature history effects as well as the coupling of rate- and temperature-dependence with material hardening. Mecking and Kocks (1981), Klepaczko and Chiem (1986), Follansbee and Kocks (1988), and Klepaczko (1988) have developed and implemented the MTS model which consists of a description of the material behavior at constant structure and a description of structure evolution during deformation. They attempted to establish a direct relation between dislocation behavior and macroscopic behavior. A reference threshold stress, $\hat{\sigma}$, is employed as the sole ISV representing a measure of the hardness of the material at its current dislocation structure. Physically, this variable represents an isotropic resistance to plastic flow which may be related to the dislocation density or dislocation substructure for single-phase, course-grained metals. The flow rule and ISV evolution equation for the uniaxial case are given by

$$\dot{\varepsilon}^p = \dot{\varepsilon}_0 \exp\left[\frac{\mu b^3 g_0}{kT}\left(1 - \left[\frac{|\sigma| - \hat{\sigma}_a}{\hat{\sigma} - \hat{\sigma}_a}\right]^p\right)^q\right]\mathrm{sgn}(\sigma) \tag{2}$$

$$\frac{d\hat{\sigma}}{d\varepsilon} = \Theta_0 \left[1 - \frac{\tan h\left(2\frac{\hat{\sigma} - \hat{\sigma}_a}{\hat{\sigma}_s - \hat{\sigma}_a} \right)}{\tan h(2)} \right] \tag{3}$$

where

$$\hat{\sigma}_s = \sigma_{s0} \left(\frac{\dot{\varepsilon}_0}{\dot{\varepsilon}_{s0}} \right)^{\left(\frac{\mu b^3 A}{kT} \right)} \tag{4}$$

The athermal stress, $\hat{\sigma}_a = \frac{0.278}{\sqrt{d}}$, which characterizes the rate independent interactions of dislocations with long-range barriers, depends on the initial average grain size, d (Gourdin and Lassila, 1991). The initial strain hardening rate, $\Theta_0 = 2150 + 0.034\dot{\varepsilon}$ is due to dislocation accumulation. This expression is obtained from a curve fit to data for OFHC with a similar initial grain size (Gourdin and Lassila, 1991). The shape of the obstacle profile is characterized by constants p and q. The normalized activation energy is g_0, $\dot{\varepsilon}_0$ is a constant restricted to $10^7 \leqslant \dot{\varepsilon}_0 \leqslant 10^{10}\,\mathrm{s}^{-1}$, k is Boltzmann's constant, b is the magnitude of the Burger's vector, μ is the shear modulus and $\dot{\varepsilon}_{s0}$ and σ_{s0} are saturation strain rate and stress at 0 K. The differential evolution equation for $\hat{\sigma}$ incorporates work hardening and dynamic recovery, but does not include either static thermal recovery or dynamic recrystallization effects. The hyperbolic tangent form for the evolution equation was chosen to approximate the Voce law such that the strain hardening rate decreases with increasing strain and approaches saturation due to dynamic recovery.

Bammann et al. (1990a), Bammann (1990), and Bammann et al. (1990b) developed the BCJ–SNL ISV constitutive model to correlate the large deformation behavior of metals. Two ISVs (a tensor kinematic hardening variable, α, and a scalar isotropic hardening variable, κ) account for the evolution of the yield surface with plastic deformation. The elastic behavior is assumed to be linear and isotropic. The flow rule and evolution equations for the uniaxial case are given by

$$\dot{\varepsilon}^p = f \sin h\left[\frac{|\sigma - \alpha| - \kappa - Y}{V} \right] \mathrm{sgn}(\sigma - \alpha) \tag{5}$$

$$\dot{\alpha} = h\mu\dot{\varepsilon}^p - [r_5 + r_d|\dot{\varepsilon}^p|]\alpha^2 \mathrm{sgn}(\alpha) \tag{6}$$

$$\dot{\kappa} = H\mu|\dot{\varepsilon}^p| - [R_s + R_d|\dot{\varepsilon}^p|]\kappa^2 \tag{7}$$

where each of the parameters f, Y, V, r_d, r_s, R_d and R_s potentially have an independent temperature dependence of the form

$$C_i \exp\left(\frac{C_j}{T}\right) \tag{8}$$

Here, the parameters h, r_d and r_s respectively describe the hardening, dynamic and static thermal recovery of the tensor or kinematic variable. Parameters H, R_d and R_s respectively describe the hardening, dynamic and static thermal recovery of the scalar or isotropic variable. Parameters f, Y and V specify the yield stress and μ is the temperature dependent shear modulus. The evolutionary equations have the form of a hardening term minus effects of both dynamic recovery and static thermal recovery. The hardening term is analogous to that proposed by Prager (1955) and represents the increase in flow resistance due to dislocation density increase with plastic deformation. The dynamic recovery term represents dislocation annihilation, cross-slip and organization into low energy structures. Note that complete recovery of state is indicated in Eqs. (6) and (7). Numerous ISV relations have been proposed analogous to this form (cf. Chaboche, 1989).

3. Parameter estimation with data correlation/predictions

A constitutive model's accuracy in predicting material behavior is not the only criterion in determining its usefulness. The practicality of using a particular model to describe material behavior also depends on the effort and skill required to determine the material parameters. Generally, a model which has physical foundations will have material parameters with a more direct interpretation than strictly empirical models. Parameters have traditionally been determined using mechanical tests combined with graphical procedures (Senseny and Fossum, 1993; Lindholm et al., 1993; Dave and Brown, 1994). Other methods include the use of expert systems such as BFIT, a program written to analyze and fit the BCJ–SNL model parameters to experimental data (Lathrop, 1996), and different optimization procedures (Braasch and Estrin, 1993; Muller and Hartmann, 1989; Sample et al., 1993). Sensitivity to parameter variation is a related issue that pertains to the degree of "uniqueness".

The typical approach to parameter evaluation is to perform a series of tests which facilitate simplified assumptions about material behavior. These assumptions are usually: (i) that the relationship between imposed stress and the inelastic strain can be measured, while the internal structure variables are constant; or (ii) that for small strain increments, the isotropic hardness does not change appreciably. Parameters are then determined graphically using the slope or changes in the slope in cross plots of variables. Senseny and Fossum (1993) found that these assumptions cannot be considered valid during most material tests due to inaccuracies in testing and because loading changes cannot be applied instantaneously. The more robust approach is to integrate the constitutive model, simulating the actual loading histories, and then use an optimization approach to evaluate the model parameters.

The optimum set of parameters necessary to describe a set of experimental data can be determined using a variety of optimization schemes. The particular constitutive model determines which of these methods will work the best in terms of

accuracy and time. Gradient, downhill simplex and genetic algorithms are three search methods to seek local minima of a multivariate level function. Parameters of a model are evaluated by minimizing an objective function which employs an error measurement. The objective function is constructed from the difference of predicted flow stress value for a particular strain level with actual measured data for the same corresponding conditions. Different error norms can be used, such as the sum of the squares of the differences (L_2 norm) or the absolute value of the greatest difference between predicted and measured data. The optimization procedure must be robust enough to handle the complicated constitutive model topology for a given set of histories. Prevalent characteristics of ISV models for inelastic behavior include strong couplings among evolution equations, high parameter sensitivity, and high mathematical stiffness. In the parameter space, the model cannot be evaluated everywhere and the objective function may be convex in some and concave in other regions.

The gradient method (Fig. 1) follows the path of the steepest gradient to the local minimum. Partial derivatives of the objective function with respect to the design parameters are calculated. This is a simple and effective method, but gets trapped in local minima (Pierre, 1969). A simplex is a body in n-dimensions consisting of $n+1$ vertices. Each vertex represents a point, consisting of a set of material parameters, in the design space. As the algorithm proceeds, the simplex makes its way downward towards the minimum location through a series of steps, called reflections, expansions, or contractions shown in Fig. 1 (Belavendram, 1995). The vertex of the simplex with the largest (worst) objective function value is moved through the opposite face to a lower point.

The genetic algorithm is useful for complex functions and large data sets and follows the mechanics of natural selection using a "generate and test" technique. A large number of points are randomly selected over the design space. Each of these points are "mutated", given a ramdom change, which produces a number of new points normally distributed around the original point. The point with the lowest objective value is then selected and is again randomly changed. Initially, this method converges rapidly and deals well with complex objective function topographies. Muller and Hartmann (1989) and Braasch and Estrin (1993) have used this evolution strategy to obtain parameters for the Hart (1976) model for 25-CrMo4 steel and Estrin (1991) model for Al-1100 aluminium, respectively.

The objective function topology determines which optimization process will be most effective in locating the global minimum and avoid getting stuck in local minima. A more powerful approach is a hybird optimization scheme which employs combinations of the gradient, simplex, and evolution techniques. Pointer Optimization Software 1.2 (Van der Velden et al., 1996) is a program which selectively uses all three optimization techniques based on evaluations of the objective function. This approach was used to determine the parameters corresponding to the Johnson/Cook, MTS, and BCJ–SNL models. For each of these three models, the parameters are determined using three constant strain rate, essentially isothermal compression experiments: 25 °C, 0.0004 s^{-1}; 269 °C, 0.1 s^{-1} and 269 °C, 0.0004 s^{-1} and two higher strain rate conditions: nominally 25 °C, 6000 s^{-1} and 269 °C, 5200 s^{-1} in which adiabatic heating effects were taken into account with a maximum temperature

increase of approximately 50 °C in both cases. These data are selected to exclude the oscillatory flow stress associated with dynamic recrystalllization, a phenomenon clearly outside the scope of these particular models. The resulting parameters are then used to calculate sequence predictions which are then compared to experimental sequence data. The sensitivity of each model's parameters is then examined. In all cases, temperature changes during the histories, including specimen insertion/removal procedures, transient heating/cooling and high strain rate excursions were taken into account in the integration of constitutive models.

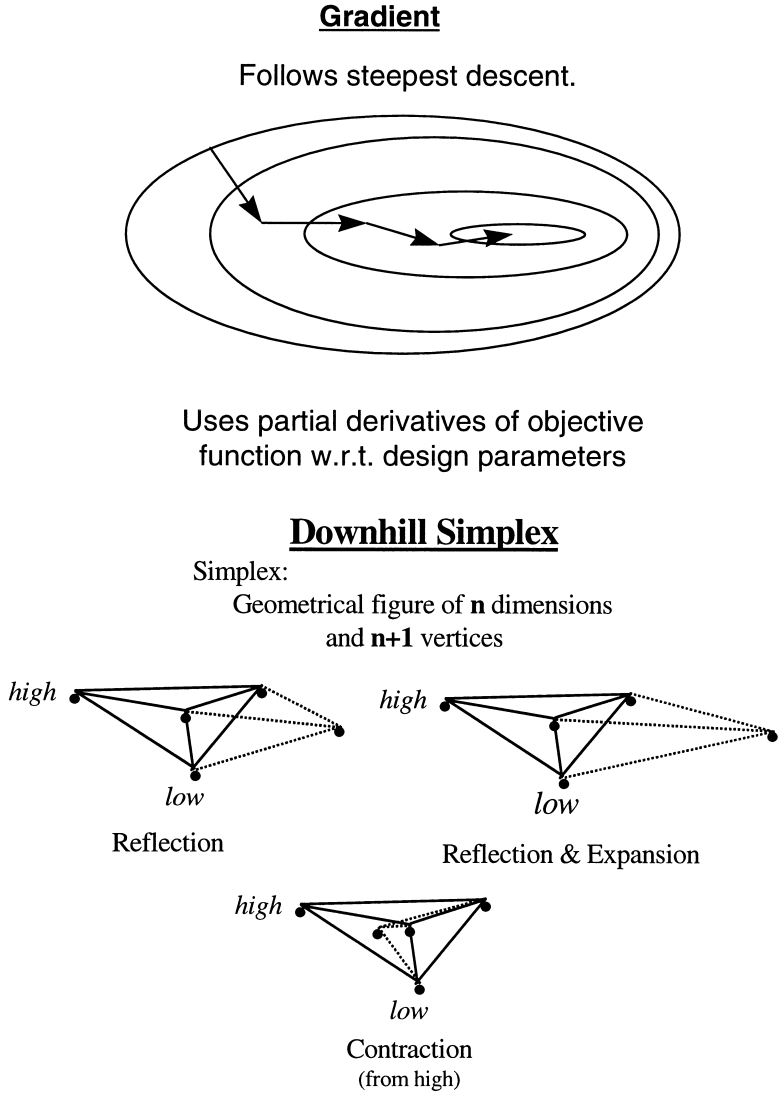

Fig. 1. Optimization schemes: gradient and downhill simplex.

Parameter sensitivity measures the effect each parameter has on the process of minimizing the objective function defined as the sum-square-errors between predicted and experimental data. The hybird optimization scheme determines the parameters set which minimizes the objective function value, $OBJ_{\text{minimized}}$. After the optimal (minimum) objective function value has been calculated, an offset in the optimal parameters is assigned. This offset, $\pm 10\%$ of all optimized parameters, results in an objective function value, OBJ_{offset}, greater than the minimum value. Additional optimizations are then conducted with the offset parameters as the initial starting condition. When all parameters are allowed to vary, the optimal objective function value, $OBJ_{\text{minimized}}$ is again achieved. The relative importance of each parameter is determined by constraining a parameter to its initial offset value. The parameter sensitivity evaluation is then based on the ability of this constrained set of parameters to achieve the minimized objective function value from the offset initial conditions during subsequent optimizations, $OBJ_{\text{constrained}}$. Parameter sensitivity is defined as

$$\eta = \text{Parameter sensitivity} = \frac{OBJ_{\text{offset}} - OBJ_{\text{constrained}}}{OBJ_{\text{offset}} - OBJ_{\text{minimized}}} \tag{9}$$

A value $\eta = 1$ results when $OBJ_{\text{constrained}} = OBJ_{\text{minimized}}$ which indicates the objective function is independent of the constrained parameter since it has no effect on achieving an optimal value of the objective function from that initial parameter offset starting location. This independence indicates the constrained parameter is not necessary to achieve the optimal objective function value and can therefore be considered redundant. A value $\eta = 0$ results when $OBJ_{\text{offset}} = OBJ_{\text{constrained}}$ which indicates the optimal objective function value is dependent on the constrained parameter. This mutual dependence incicates the constrained parameter is essential to achieving the optimal objective function value. Two sets of parameter sensitivity evaluations are made. The first measures the ability of one parameter to achieve the optimal objective function value with all other parameters constrained. Additionally, the sensitivity is determined from the ability of all the other parameters, without the single or set of parameters, to reach the minimized objective.

3.1. Johnson/Cook model

The Johnson/Cook model (Johnson and Cook, 1983) has five parameters (σ_0, B, C, n, and m) which are determined using data for large strain, constant true strain rate compression experiments, resulting in the correlation shown in Fig. 2. The temperature rise of the high strain rate experiments was recorded and accounted for in modeling. Temperature and strain rate dependence is predicted, but not the actual strain hardening or dynamic softening. The optimized parameter values are shown in Table 1, with other parameters calculated for OFHC Cu.

3.1.1. Johnson/Cook model sequence predictions

Predictions are calculated using the optimized parameters for the Johnson/Cook model for compression tests involving strain rate sequences (Figs. 3 and 4), temperature

sequences (Figs. 5 and 6) and for combined strain rate and temperature sequences (Figs. 7 and 8). The solid lines represent the model prediction, while symbols represent experimental data. The Johnson/Cook model does not predict any history effects. During the predicted sequences, the flow stress changes instantaneously from the flow stress associated with the initial set of conditions to that associated with the next. No transition behavior is predicted, consistent with the form of the model.

3.1.2. Johnson/Cook model parameter sensitivity

A parameter sensitivity study was completed for the Johnson/Cook model using the optimized values shown in Table 1. The light and dark bars in Fig. 9 reflect $\pm 10\%$ offset from optimized values. The first two bars reflect the ability of the indicated parameter alone to achieve the global minimum while the second two bars show how the well the remaining parameters can reach the minimum with the indicated parameter held constant. This analysis shows that any one of the five parameters can be held constant and the optimized objective function value can still be achieved. The model's performance is most sensitive to the m parameter.

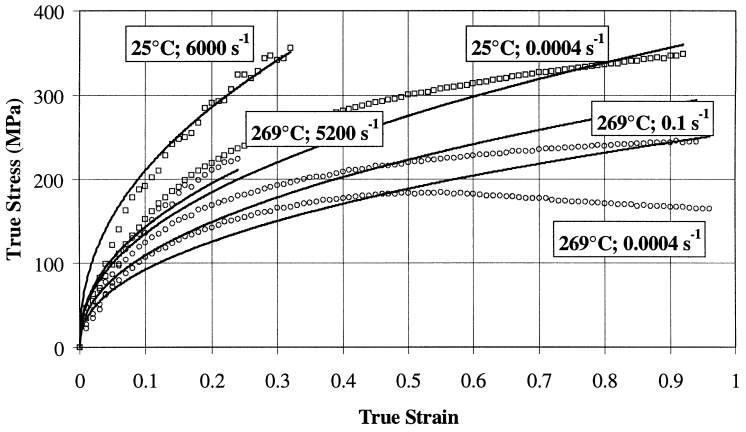

Fig. 2. Correlation to OFHC Cu data using Johnson/Cook model. The model correlations are shown using solid lines, while the experimental data are shown with open symbols.

Table 1
Johnson/Cook model parameter comparison for OFHC Cu

Parameter	(Johnson and Cook, 1983)	Optimized
Deformation conditions	10^3 to $10^5\,s^{-1}$	4×10^{-4} to $6\times10^3\,s^{-1}$ 25 to 269 °C 62 μm
σ_0 (MPa)	90	0
B (MPa)	292	470
C	0.025	0.027
n	0.31	0.44
m	1.09	0.78

3.2. MTS model

The threshold $\hat{\sigma}$, is the flow stress of the material, for a given internal structure, at 0 K. This is the stress required to overcome obstacles in the absence of any contribution from thermal activation energy. The threshold stress characterizes the strength and density of obstacles. The material flow stress is the combination of the stress required to overcome the dynamically generated barriers reduced by the thermal activation energy. The eight parameters (g_0, p, q, k/b^3, A, $\dot{\varepsilon}_0$, $\dot{\varepsilon}_{s0}$, and σ_{so}) used in the MTS model are obtained using the same five constant true strain rate compression tests as before. Constraints were imposed on several parameters. The constants p and q, which define the average obstacle profile, are restricted to $0 \leqslant p \leqslant 1$ and

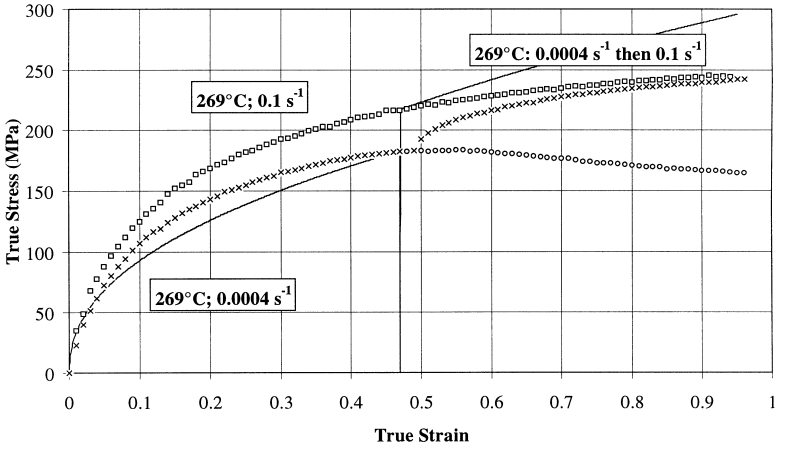

Fig. 3. Strain rate sequence prediction for OFHC Cu using the Johnson/Cook model. Solid lines represent the model prediction, while symbols represent data.

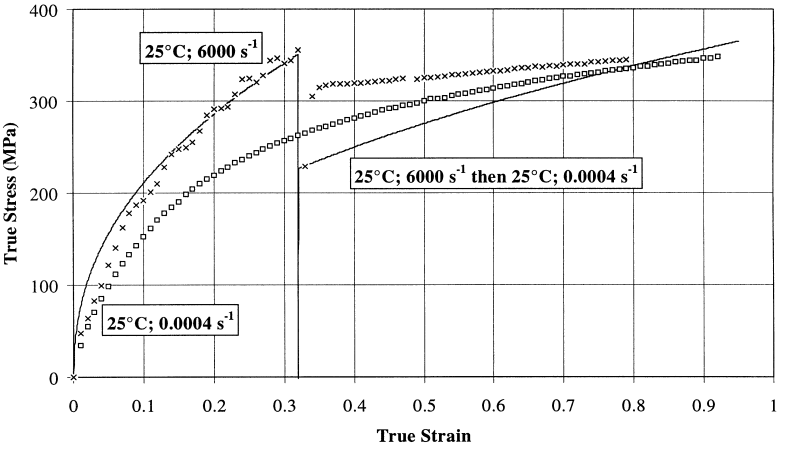

Fig. 4. Strain rate sequence prediction for OFHC Cu using the Johnson/Cook model. Solid lines represent the model prediction, while symbols represent data.

$1 \leqslant q \leqslant 2$ (Kocks et al., 1975) and the constant $\dot{\varepsilon}_0$, is limited to values $10^7 \leqslant \dot{\varepsilon}_0 \leqslant 10^{10}\,\mathrm{s}^{-1}$ (Johnson, 1988). The correlation to the five data sets are shown in Fig. 10. The model correlates the data well, except for the strain softening observed at 269 °C at a strain rate of $0.0004\,\mathrm{s}^{-1}$.

Table 2 shows a comparison of the optimized parameter values with other values determined using a graphical approach. The values are reasonably consistent, providing confidence that the physical interpretation of the parameters is valid. The parameter, $\dot{\varepsilon}_{s0}$, is many orders of magnitude different than previously determined values. This term is used to obtain the saturation stress value in Eq. (4). The parameter is embedded within a logarithmic term and is coupled with parameters $A, k/b^3$ and σ_{so}, so is not necessary to determine a precise value (Johnson, 1988).

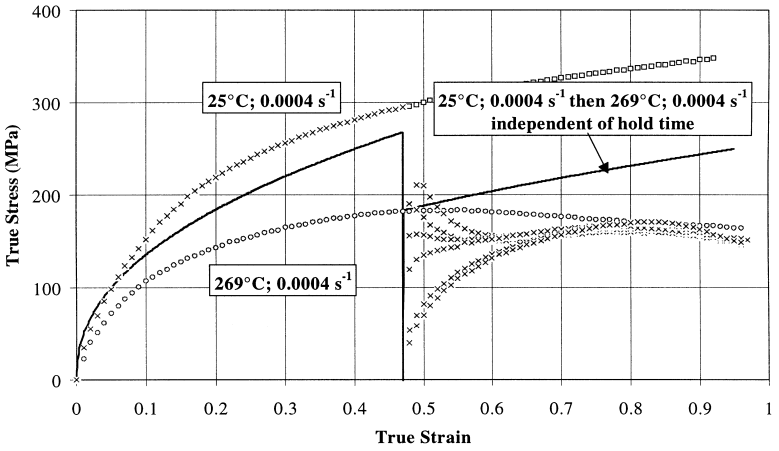

Fig. 5. Temperature sequence prediction for OFHC Cu using the Johnson/Cook model. Solid lines represent the model prediction, while symbols represent data.

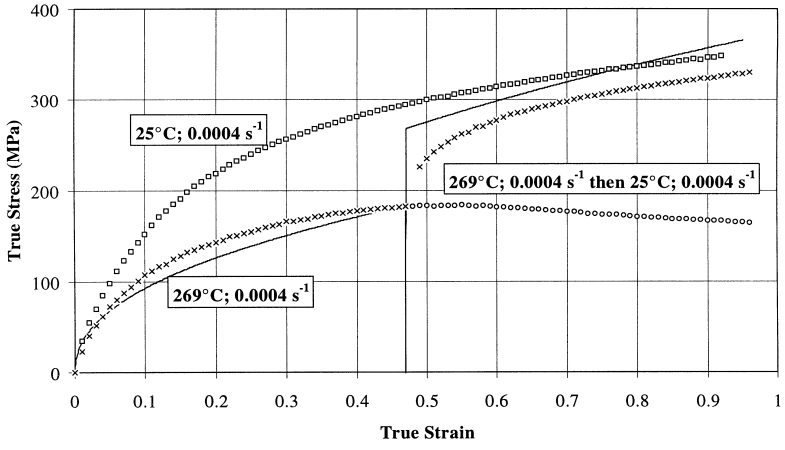

Fig. 6. Temperature sequence prediction for OFHC Cu using the Johnson/Cook model. Solid lines represent the model prediction, while symbols represent data.

3.2.1. MTS Model sequence predictions

Predictions using the optimized parameters for the MTS model are shown for the strain rate sequence results (Figs. 11 and 12), temperature sequence results (Figs. 13 and 14), and combined strain rate and temperature sequence results (Figs. 15 and 16).

The MTS model lacks capability to describe restoration processes such as diffusional thermal recovery or recrystallization and associated strain softening (Figs. 13 and 15). It predicts the response rather well for strain rate and temperature sequences excluding static thermal recovery effects. Since it has no kinematic hardening and a single hardening variable, the MTS model is limited in ability to capture details of transients just after a change in loading condition.

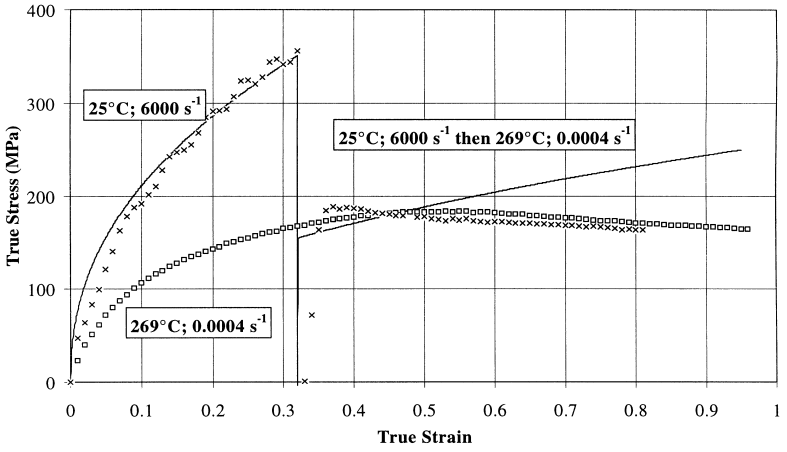

Fig. 7. Strain rate and temperature sequence prediction for OFHC Cu using the Johnson/Cook model. Solid lines represent the model prediction, while symbols represent data.

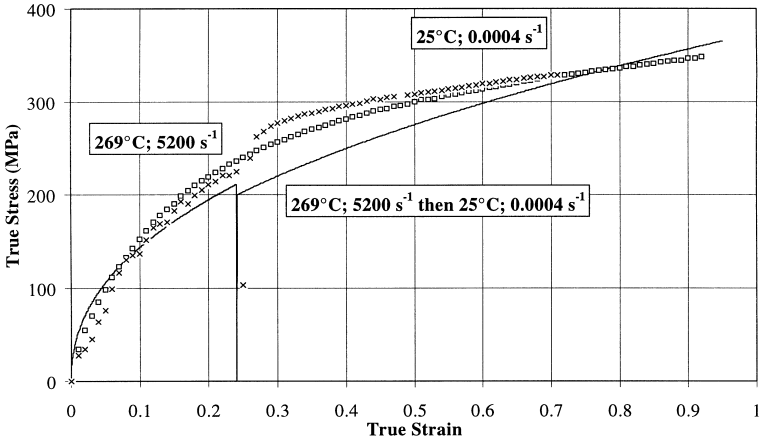

Fig. 8. Strain rate and temperature sequence prediction for OFHC Cu using the Johnson/Cook model. Solid lines represent the model prediction, while symbols represent data.

3.2.2. MTS model parameter sensitivity

A parameter sensitivity study was conducted for the MTS model using the optimized values shown in Table 2. The light and dark bars in Fig. 17 reflect ±10% offset from optimized values. This analysis indicates that there is redundancy in the parameters, since any one of the eight can be held constant and the optimized objective function value can still be practically achieved. Parameter σ_{so} is the only

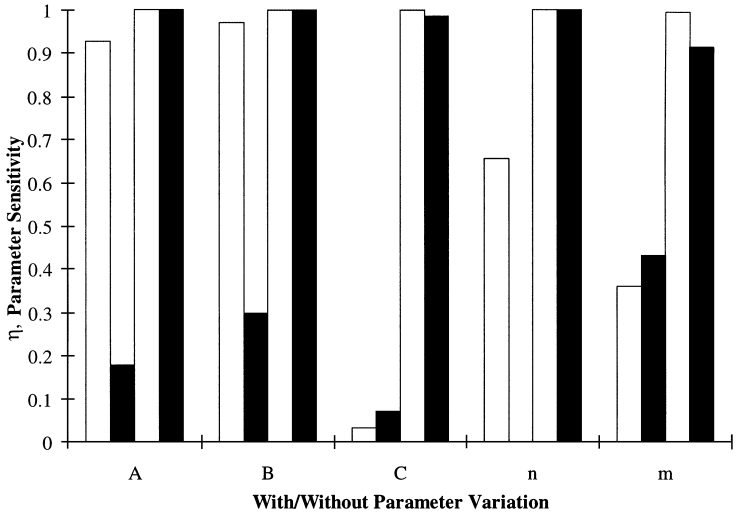

Fig. 9. Parameter sensitivity for OFHC Cu using the Johnson/Cook model. Light and dark bars reflect a ±10% offset from the optimized parameter values corresponding to a minimum of the objective function. First two bars show ability of indicated parameter, alone, to achieve the global minimum while the second two bars show ability of the remaining parameters, with the indicated parameter held constant, to reach the minimum.

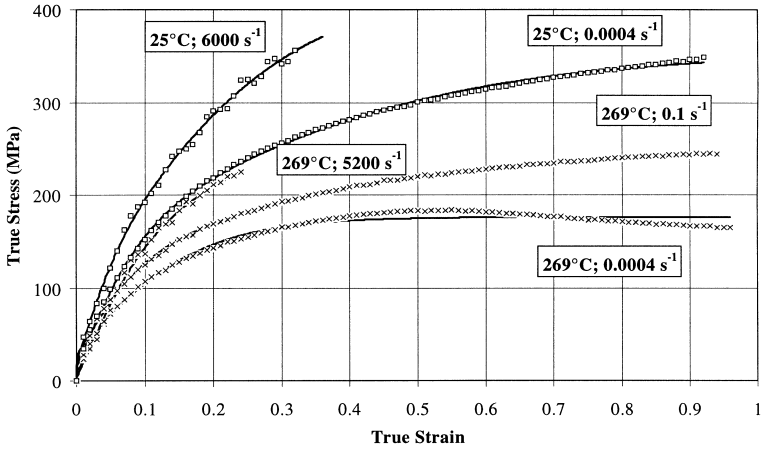

Fig. 10. Correlation to OFHC Cu compression data using the MTS model. The model correlations are shown using solid lines, while the experimental data are shown with open symbols.

one which has much impact by itself on achieving the minimum error. k/b^3 has the least capability to reduce the objective function, so has the least sensitivity.

3.3. BCJ–SNL model

The BCJ–SNL model employs nine parameters. The first three are V, Y and f which specify the flow stress relative to α, the kinematic hardening variable, with Y controlling the rate independent part and V and f controlling the rate dependent part. Parameters h, r_d, and r_s describe the evolution of α, including direct hardening, dynamic recovery, and static thermal recovery, respectively. Similarly, H, R_d and R_s govern the evolution of the isotropic variable, κ. The nine parameters all have a temperature dependence, V, f, Y, r_d, r_s, R_d, and R_s through a form as described in Eq. (8) and h and H through a coupling with the modulus,

Table 2
MTS model parameter comparison for OFHC Cu

Parameter	Follansbee and Kocks (1988)	Gourdin and Lassila (1991)	Optimized
Deformation conditions	10^{-4} to $10^{4}\,s^{-1}$ 25 °C 40 μm	10^{-3} to $10^{4}\,s^{-1}$ 25 to 400 °C 10–200 μm	4×10^{-4} to $6\times10^{3}\,s^{-1}$ 25 to 269 °C 62 μm
g_0	1.6	1.6	2.98
p	2/3	2/3	0.318
q	1.0	1.0	1.20
$\dot{\varepsilon}_0$ (s^{-1})	10^7	10^7	10^7
k/b^3 (MPa K^{-1})	0.823	0.823	0.848
A	0.31	0.235	0.633
σ_{so} (MPa)	900	1100	1070
$\dot{\varepsilon}_{s0}$ (s^{-1})	6.2×10^{10}	5.66×10^{10}	4.0×10^{23}

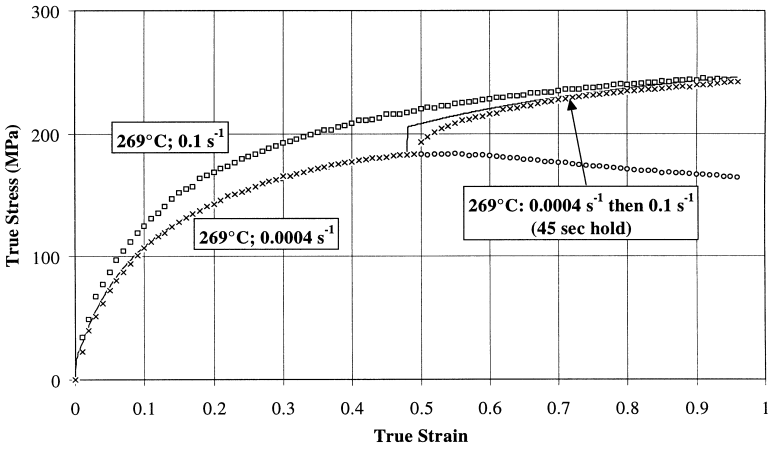

Fig. 11. Strain rate sequence prediction for OFHC Cu using the MTS model. Solid lines represent the model prediction, while symbols represent experimental data.

$$\mu = \mu_0\left[1 - \left(\frac{T}{T_m}\right)\exp\left[T_0\left(1 - \frac{T}{T_m}\right)\right]\right] \tag{10}$$

where T_0 is the reference temperature for μ_0. The nine parameters ($V, f, Y, r_d, h, r_s, R_d, H$, and R_s) are obtained using the same five isothermal, constant strain rate conditions as for the other models. An initial value of zero was used for both α and κ for the initially annealed material. An apparent softening can be achieved when a negative initial value for κ is assumed. The correlations with the five data sets are shown in Fig. 18. The data are well correlated with experimental data, except for the strain softening observed at 269 °C above 0.5 strain.

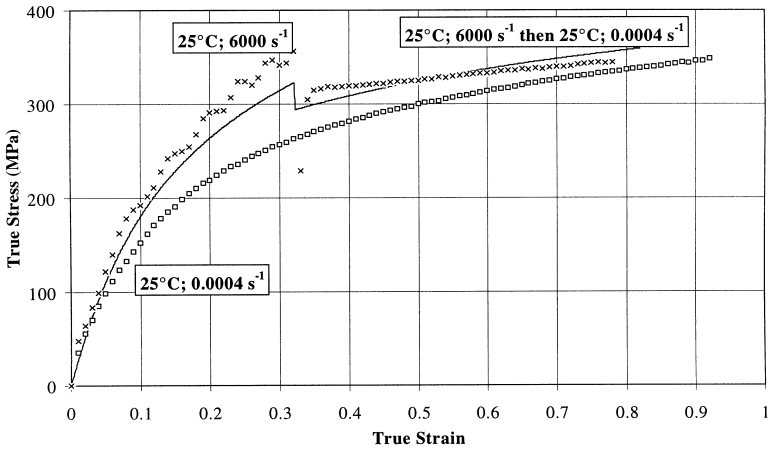

Fig. 12. Strain rate sequence prediction for OFHC Cu using the MTS model. Solid lines represent the model prediction, while symbols represent experimental data.

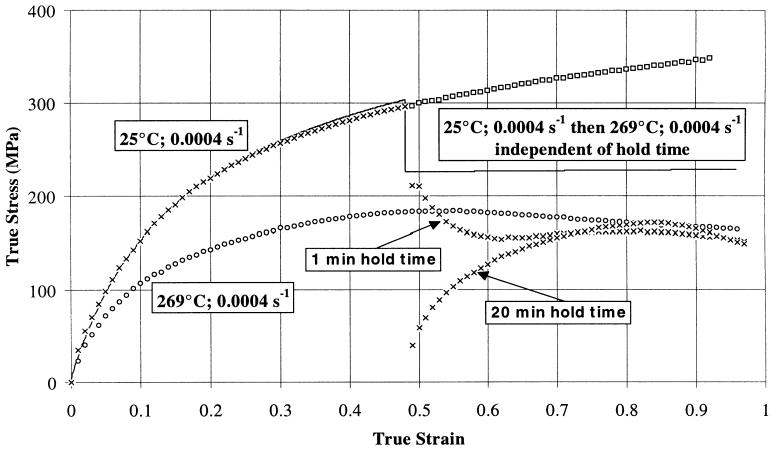

Fig. 13. Temperature sequence prediction for OFHC Cu using the MTS model. Solid lines represent the model prediction, while symbols represent experimental data.

The ratio of the magnitude of the kinematic to the isotropic hardening ISVs ($|\alpha|/\kappa$) is also shown on each plot for each case as short dashed curves. The saturation ratio at large strain was constrained in the optimization process to be between 0.05 and 0.3. This range of values is consistent with the experimentally determined value for OFHC Cu using a reverse loading path of 0.22 (Jackson et al., 1997). The kinematic hardening variable accounts for short range work hardening transients and the isotropic the longer range transients. This ratio is seen to increase for increasing strain rates. Predictions using the optimized parameters for the BCJ–SNL model are shown in Figs. 19 and 20 for strain rate sequence experiments, Figs. 21 and 22 show the temperature sequence results, and Figs. 23 and 24 show combined strain rate and temperature sequence results. In Fig. 21, the zero applied stress hold

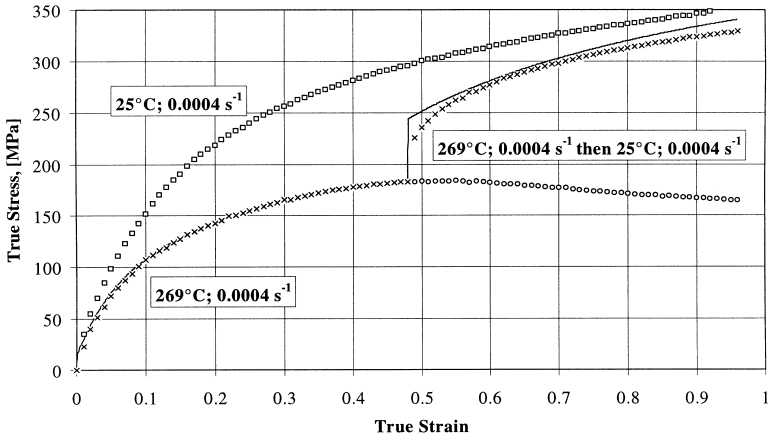

Fig. 14. Temperature sequence prediction for OFHC Cu using the MTS model. Solid lines represent the model prediction, while symbols represent experimental data.

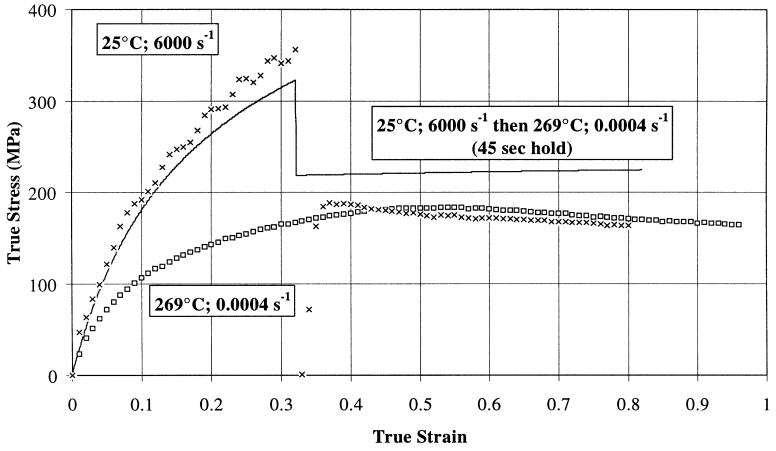

Fig. 15. Strain rate and temperature sequence prediction for OFHC Cu using the MTS model. Solid lines represent the model prediction, while symbols represent experimental data.

period (delay) used in the modeling was 20 min. In all cases, the ratio of kinematic to isotropic hardening is plotted as a function of strain. The initial ratio is the same in all cases (1.13), corresponding to the ratio of direct hardening coefficients, h/H. It is clear that description of transient history effects is enhanced by the introduction of the two ISVs (Table 3).

The BCJ–SNL model incorporates many of the observed history effects. However, there is insufficient restoration of state in the model while holding at zero applied stress at 269 °C in-between loading events (Figs. 19 and 22). Likewise, the reader should recall the under-predicted restoration in Fig. 21. It is also dominately a consequence of the neglect of recrystallization in this model, as understood by a more comprehensive experimental study and modeling treatment of restoration processes (Tanner, 1998). Moreover, no stress relaxation or creep data were used in parameter

Table 3
BCJ–SNL optimized model parameters for OFHC Cu for strain rates 4×10^{-4} to $6\times10^{3}\,s^{-1}$ and temperatures 25 to 269 °C

Parameter	Optimized value
Deformation conditions	4×10^{-4} to $6\times10^{3}\,s^{-1}$, 25 to 269 °C, 62 μm
V	10^{-6} (−43)
Y	1.7 (70)
f	38 (−15)
r_d	0.15 (−12)
h	0.024
r_s	0.046 (−120)
R_d	0.028 (−22)
H	0.021
R_s	10^{-9} (−130)

The temperature dependence parameter C_j, is provided in parentheses.

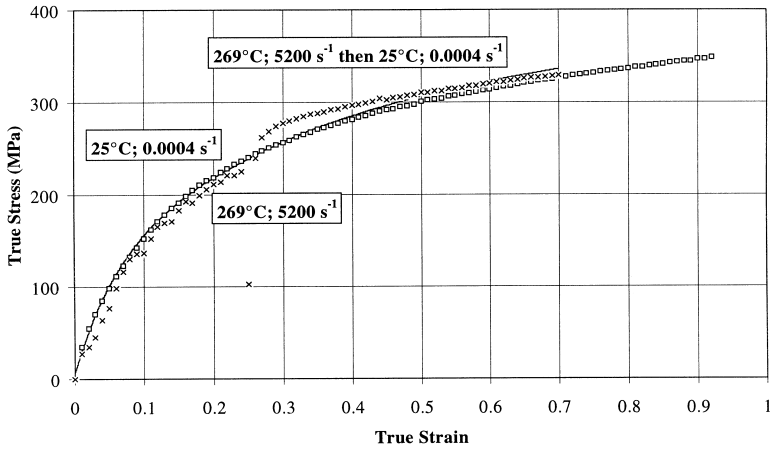

Fig. 16. Strain rate and temperature sequence prediction for OFHC Cu using the MTS model. Solid lines represent the model prediction, while symbols represent experimental data.

estimation which leads to an inaccurate estimation of static thermal recovery terms in the model; preferably, data would also exclude recrystallization processes to isolate the static thermal recovery effects. Strain softening at 269 °C following dynamic pre-strain is also not predicted (Fig. 23); the model does not have this capability given its asymptotic saturation for a given temperature and strain rate.

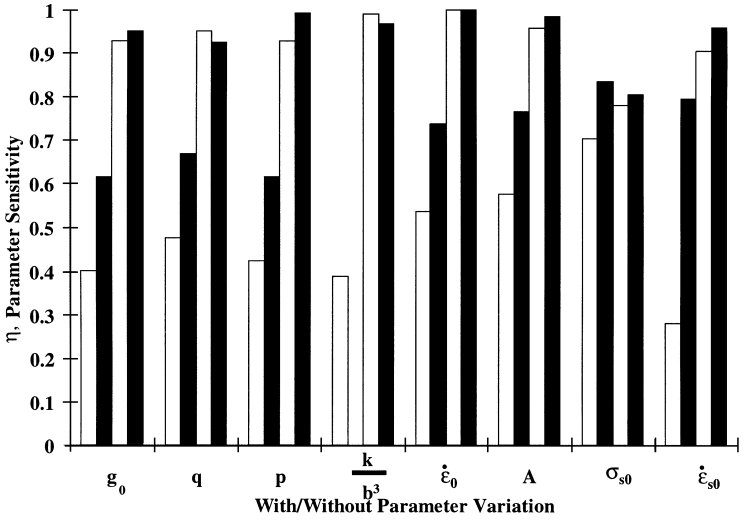

Fig. 17. Parameter sensitivity for OFHC Cu using the MTS model. Light and dark bars reflect a ±10% offset from the optimized parameter values corresponding to a minimum of the objective function. First two bars show ability of indicated parameter, alone, to achieve the global minimum while the second two bars show ability of the remaining parameters, with the indicated parameter held constant, to reach the minimum.

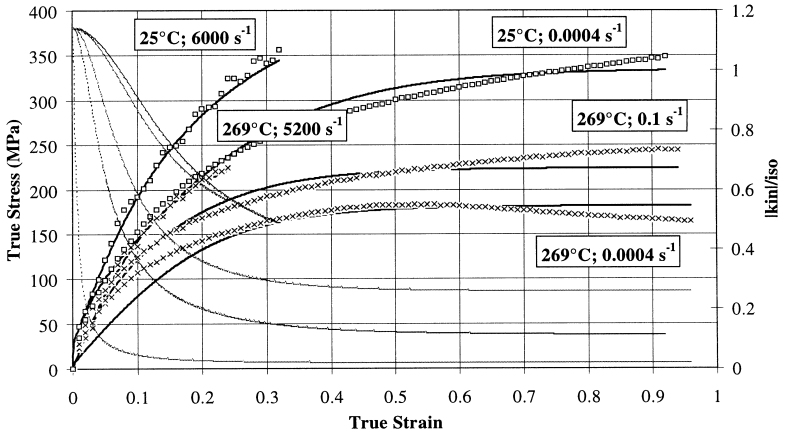

Fig. 18. Correlation to OFHC Cu compression data using the BCJ–SNL model. The model correlations are shown using solid lines, while the experimental data are shown with open symbols. The ratio $|\alpha|/\kappa$ are displayed using short dashed lines.

3.3.1. BCJ–SNL model parameter sensitivity

Figure 25 shows the results of BCJ–SNL model parameter sensitivity study. The parameter sensitivity analysis shows that the hardening variables h and H are the most critical parameters to achieving the optimal objective (lowest error) function. It also, indicates that there is redundancy in the three yield variables, V, f and Y. Alone, none of these functions have much impact on achieving the minimum error (a zero value), but combined (yield), they are effective. The analysis also shows that the recovery terms, both static and dynamic, are essential; the optimal error cannot be attained without them by varying other parameters.

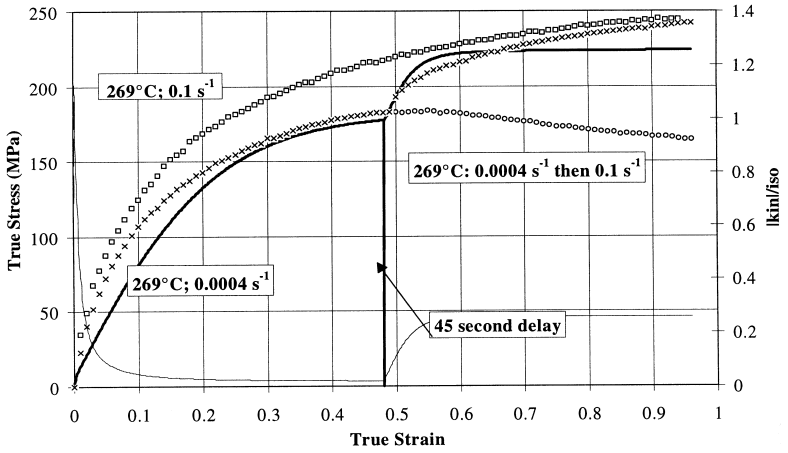

Fig. 19. Strain rate sequence prediction for OFHC Cu using the BCJ–SNL model. Solid lines represent the model prediction, while symbols represent experimental data.

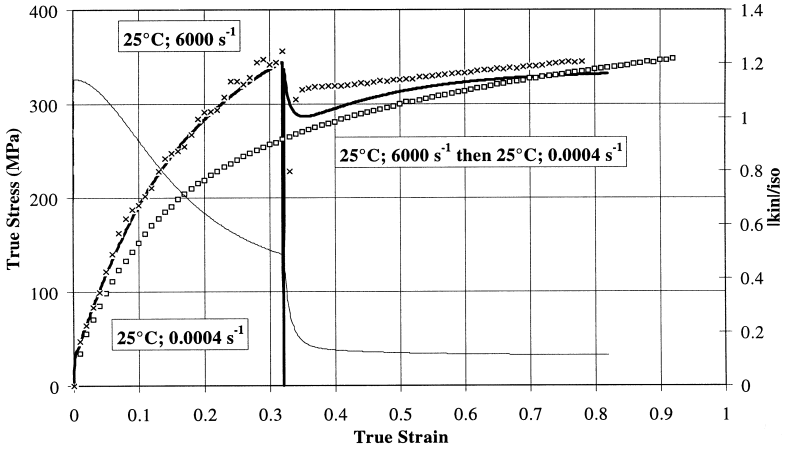

Fig. 20. Strain rate sequence prediction for OFHC Cu using the BCJ–SNL model. Solid lines represent the model prediction, while symbols represent experimental data.

4. Discussion

OFHC Cu exhibits many macroscopic characteristics which models must capture to accurately predict material response. These include the primary material dependencies on temperature and strain rate and, additionally, dynamic softening, resulting in an actual reduction in flow stress at 269 °C, static recovery and both temperature and strain rate history effects. As the predictive accuracy requirements for models have increased, so has the need to include these additional features.

Flow stress is not only a function of instantaneous values of strain, strain rate and temperature, but exhibits transients and in some cases different asymptotic flow

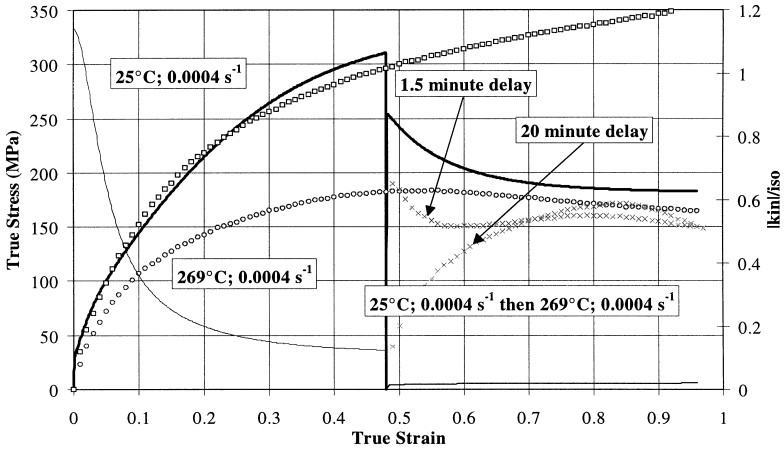

Fig. 21. Temperature sequence prediction for OFHC Cu using the BCJ–SNL model. Solid lines represent the model prediction, while symbols represent experimental data.

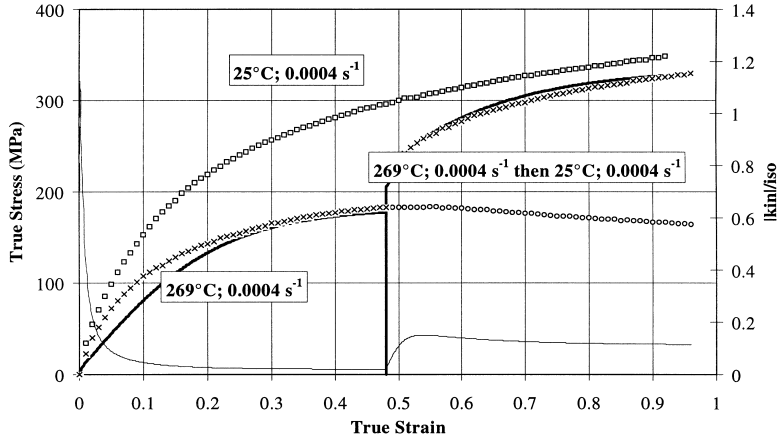

Fig. 22. Temperature sequence prediction for OFHC Cu using the BCJ–SNL model. Solid lines represent the model prediction, while symbols represent experimental data.

stress levels. A mechanical equation-of-state model clearly cannot capture these sequence effects. The empirical Johnson/Cook constitutive model correlates the primary temperature and strain rate dependencies in OFHC Cu, but does not have the capability to predict sequence effects. The instantaneous response of a material depends on its current state, which in turn depends on the entire history of deformation. The MTS and BCJ–SNL models utilize one and two internal variables, respectively. The ISV evolutionary equations account for prior deformation and permit transient flow stress behavior to be modeled. The BCJ–SNL model, with two internal variables, has an enhanced predictive capability relative to the MTS model for sequence effects.

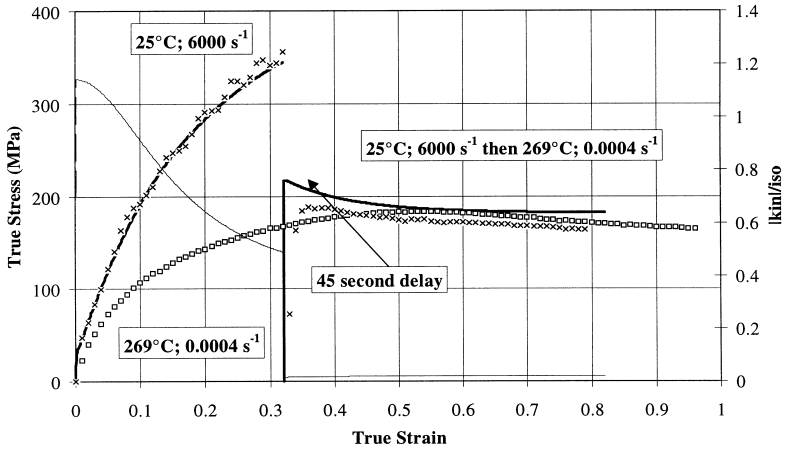

Fig. 23. Strain rate and temperature sequence prediction for OFHC Cu using the BCJ–SNL model. Solid lines represent the model prediction, while symbols represent experimental data.

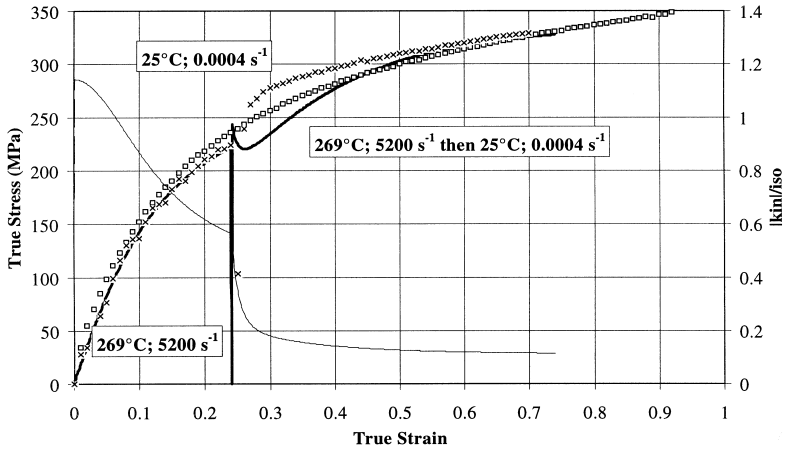

Fig. 24. Strain rate and temperature sequence prediction for OFHC Cu using the BCJ–SNL model. Solid lines represent the model prediction, while symbols represent experimental data.

OFHC Cu demonstrates significant softening due to restoration of internal structure at 269 °C. The MTS model considered here does not contain any static thermal recovery or recrystallization terms, so does not predict any recovery while holding at elevated temperature (Figs. 11–13). The BCJ–SNL model contains static thermal recovery in both α and κ evolution equations and does predict some recovery (Figs. 19 and 21), but the amount of restoration is under-predicted (Fig. 21). The isotropic static thermal recovery parameter magnitude, R_s, was too small as a result of using data from only constant strain rate, nominally isothermal experiments for determining the parameters. The static thermal recovery terms incorporated in the BCJ–SNL model result in improved prediction of the transients occurring at 269 °C. Both models best predict temperature decrease sequences, 269 °C to 25 °C at $0.0004\,s^{-1}$ (Figs. 14 and 22), since little or no restoration of internal structure occurs at 25 °C (McQueen and Jones, 1975).

OFHC also exhibits dynamic strain softening at 269 °C, which is largely due to dynamic recrystallization (Tanner, 1998). The greatest error associated with the correlation of both macroscale ISV models with the constant strain rate data results from neither model accounting for the softening of flow stress at 269 °C. The evolutionary equations for both models saturate to zero rate. Consequently, the MTS model predicts a transient behavior which demonstrates an initial sharp increase or decrease in flow stress, remaining between the two constant temperature and/or strain rate curves (Figs. 11–15), rather than an asymptotic approach to the higher constant temperature and/or strain rate curve (Figs. 11, 12 and 14) or an immediate saturation in flow stress (Figs. 13 and 15). The immediate saturation is due the structure of the evolution equation for the ISV, $\hat{\sigma}$, which remains positive during an unloading process.

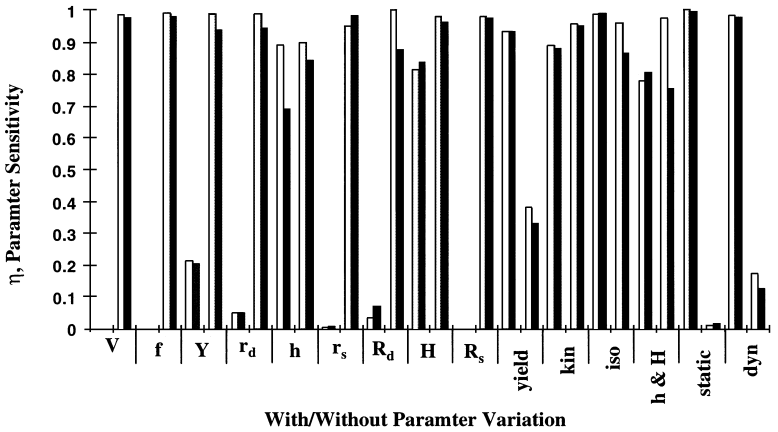

Fig. 25. Parameter sensitivity for OFHC Cu using the BCJ–SNL model. Light and dark bars reflect a ±10% offset from the optimized parameter values corresponding to a minimum of the objective function. First two bars show ability of indicated parameter, alone, to achieve the global minimum while the second two bars show ability of the remaining parameters, with the indicated parameter held constant, to reach the minimum.

Static thermal recovery and recrystallization processes must be included to accurately predict OFHC Cu response. Capturing these features may not be fully sufficient, though. Internal stresses in a material are created by many different obstacles to dislocation motion. They have a variety of shapes and resistances and have typically been categorized as short or long range. Peierls barriers and forest dislocations are relatively weak obstacles which can be overcome with the assistance of thermal activation. Strong obstacles to dislocation motion are cell walls, grain boundaries, twins, etc. The effects of long range internal stresses can be distinguished from those of short range by their respective slow and fast kinetics (Lowe and Miller, 1986). A single internal state variable cannot account for these different kinetics. It is clear that the inclusion of a short range kinematic hardening variable in the BCJ–SNL model is able to predict transients significantly better than a formulation with just a single isotropic hardening variable. Furthermore, the evolution of the ratio of kinematic to isotropic hardening variables in the BCJ-SNL model reveals both strain rate and temperature dependence in the monotonic loading responses in addition to rapid transients following abrupt changes of temperature, strain rate or deformation path. This ratio increases significantly with an increase strain rate at a given temperature for the BCJ–SNL model.

The optimization procedure seems particularly effective in obtaining a parameter set which results in the best fit to experimental data. The objective function was defined as the minimization of the error norm based on the sum of the square of the differences between predicted and actual data. The optimized error norms for each model are shown in Table 4. The error value using parameter sets obtained using the traditional graphical technique is compared to that obtained using the optimized parameters. The optimized values all produced much smaller error norms.

The results of this section have demonstrated the roles of restoration and splitting of the ISVs into short and long range components in a macroscale formulation. It is of interest to explore how these results may carry over to the case of increased order of ISVs in a mesoscale description. In the next section, a continuum slip polycrystal plasticity model is employed to investigate the effect of partitioning the slip system hardening variable into short and long range components. Although macroscale yield surfaces have been proposed for a given state of texture [see Maudlin et al. (1995) for the MTS model extension], the polycystal plasticity treatment offers the most general setting for capturing texture evolution.

Table 4
Comparison of error norm (normalized to smallest value)

	Traditional technique	Optimized
Johnson/Cook	9200	5.3
MTS	2.4[a] 4.0[b]	1.5
BCJ-SNL		1.0

[a] Follansbee and Kocks, 1988.
[b] Gourdin and Lassila, 1991.

5. Polycrystal plasticity

A polycrystal plasticity model was employed to evaluate the ability of a continuum crystallographic slip mesoscale model with the capability of modeling evolution of crystallographic texture to reproduce the transient stress–strain curves associated with temperature sequence tests. The mesoscale approach permits the introduction of hardening laws at the slip system level of the grain as compared to the macroscale approaches which address collective polycrystal behavior in an average sense. We may sort out effects of intergranular constraint and slip system hardening on the response under sequence loadings described in the previous sections. The polycrystal plasticity model has a fully implicit 3-D elastic-plastic finite deformation rate-based formulation with Taylor (1938) constraints. It is implemented in ABAQUS/IMPLICIT (Hibbitt et al., 1997) using the algorithm of Cuitino and Ortiz (1992). The predictions employ the average response of 200 grains comprising an initially random orientation distribution (texture). The orientation vectors for slip planes may be regarded as additional mesoscale ISVs. The flow rule is assumed as

$$\dot{\gamma}^{(\alpha)} = 0.001\left|\frac{\tau^{(\alpha)}}{g^{(\alpha)}}\right|^{10} \operatorname{sgn}\left(\tau^{(\alpha)}\right) \tag{11}$$

where $\dot{\gamma}^{(\alpha)}$ is the shear strain rate, $\tau^{(\alpha)}$ is the resolved shear stress, and $g^{(\alpha)}$ is a reference shear stress of the αth slip system. As the history to be modeled here was conducted at a constant strain rate, we adopt a value of strain rate sensitivity which results in a less mathematically stiff relations for purposes of numerical integration, not necessarily representative of the actual value for OFHC Cu. The hardening law for $g^{(\alpha)}$ is assumed to include conventional direct hardening and dynamic recovery, i.e.

$$\dot{g}^{(\alpha)} = H_{\mathrm{dir}} \sum_{\beta=1}^{N} |\dot{\gamma}^{(\beta)}| - R_{\mathrm{dyn}} g^{(\alpha)} \sum_{\beta=1}^{N} |\dot{\gamma}^{(\beta)}| \tag{12}$$

where H_{dir} is a direct hardening constant, R_{dyn} is a dynamic recovery constant and N is the number of octahedral slip systems (in this case, $N = 12$). In this implementation of the model, we do not consider kinematic hardening at the level of the individual slip system, although the intergranular constraint relation and orientation distribution of grains will introduce some level of Bauschinger effect.

The model was applied to two sets of experimental temperature sequence data for compression of OFHC Cu. The temperature change was from 25 to 269 °C at the same compressive strain rate. The data for the temperature change are shown in Figs. 26 and 27, respectively, along with model predictions that will be discussed next.

The model, with one hardening variable, was independently fit to the 25 °C and the 269 °C constant strain rate data. The resulting parameter evolution equations for the hardening variable, g, are given by $H_{\mathrm{dir}} = 225$, $R_{\mathrm{dyn}} = 2$ at 25 °C and $H_{\mathrm{dir}} = 150$, $R_{\mathrm{dyn}} = 2.3$ at 269 °C.

Equations (11) and (12) were used to evaluate how well the model predicts the temperature sequence data. Figure 26 shows that the accuracy of the predicted transient response is rather poor. Compared to the experimental data, the evolution of stress after the temperature decrease at 50% compression is too slow, but then overshoots the experimental flow stress later. This inaccuracy is believed to be due to the inability of a single hardening variable to account for both long and short range obstacles.

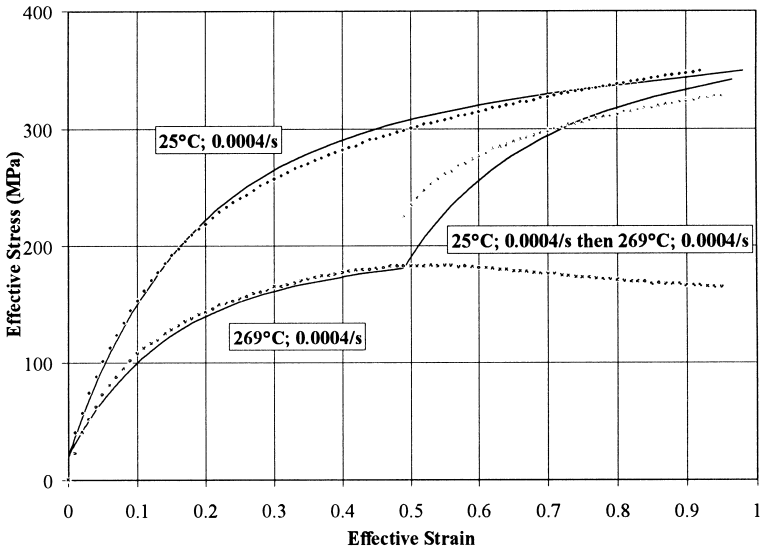

Fig. 26. Temperature sequence prediction using one hardening variable.

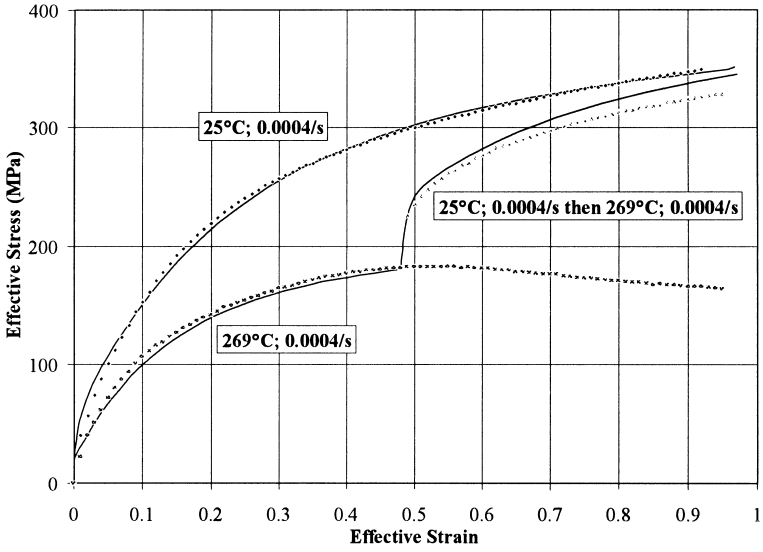

Fig. 27. Temperature sequence prediction using the hardening variables.

A variation of the above hardening law was also examined. The hardening variable, $g^{(\alpha)}$, was partitioned into a linear sum of hardening variables, $g_i^{(\alpha)}$, each with a hardening law, i.e.

$$\dot{g}^{(\alpha)} = \sum_{i=1}^{2} \dot{g}_{(i)}^{(\alpha)} \text{ with } \dot{g}_{(i)}^{(\alpha)} = H_{\text{dir}}^{i} \sum_{\beta=1}^{N} |\dot{\gamma}^{(\beta)}| - R_{\text{dyn}}^{i}\, g_{(i)}^{(\alpha)} \sum_{\beta=1}^{N} |\dot{\gamma}^{(\beta)}|. \tag{13}$$

Here $g_{(i)}^{(\alpha)}$ represents short range effects such as dislocation–dislocation interactions and is expected to saturate quickly; $g_{(2)}^{(\alpha)}$ represents long range, slowly evolving effects such as dislocation interactions with grain boundaries and sub-grain boundaries. The second term, $g_{(2)}^{(\alpha)}$, is expected to saturate more slowly.

Figure 27 shows the results of fitting the modified model to the data. It can be seen that incorporation of two hardening variables has improved model accuracy for this two-temperature sequence. The high hardening rate just after the temperature decrease reflects the rapid increase in short range obstacles. This effect saturates quickly, leaving the more slowly evolving long range mechanisms to control the hardening rate thereafter. The hardening parameters are given by $H_{\text{dir}}^{1} = 1000$, $R_{\text{dyn}}^{1} = 50$, $H_{\text{dir}}^{2} = 150$, $R_{\text{dyn}}^{2} = 1.6$ at 25 °C; $H_{\text{dir}}^{1} = R_{\text{dyn}}^{1} = 0$, $H_{\text{dir}}^{2} = 150$, $R_{\text{dyn}}^{2} = 2.3$ at 269 °C. This result, based on the hardening law at the individual slip system level, reinforces the need to introduce both short and long range transient hardening variables.

6. Conclusions

This paper investigates parameter estimation of two ISV constitutive models across a range of temperatures and strain rates for finite straining of OFHC Cu. Using the parameter sets determined by fitting constant strain rate compression tests, the capability of three constitutive models to accurately predict sequence history effects was studied. Additionally, a polycrystal plasticity model was examined. Temperature changes during all parts of the histories were recorded and taken into account in the time integration of models.

The capability of two ISV models to predict temperature and strain rate history effects was compared to the Johnson/Cook equation-of-state model. The evolutionary internal state variables permit history effects to be predicted. However, the current models do not accurately capture all the transients. The BCJ–SNL model, with both kinematic and isotropic internal hardening variables, is somewhat more comprehensive in its treatment of restoration effects, both dynamic and static thermal recovery, which may account for its enhanced predictive capability relative to the MTS model. The latter does not include static thermal recovery effects. Neither model describes recrystallization processes and associated softening of the flow stress. Neither has a temperature rate term which may limit the capability to account for nonisothermal behavior (cf. McDowell, 1992). The incorporation of two hardening variables in the polycrystal plasticity model improved the ability to accurately describe the transient behavior for a temperature sequence compression experiment.

This allocation of hardening into short range and long range variables seems to offer more accurate description of actual behavior, and kinematic hardening plays a distinct role in the short range transients.

Constitutive equation material parameters for OFHC Cu experimental data are estimated using a non-linear, constrained optimization procedure (Van der Velden et al., 1996). This procedure, using a combination of genetic, gradient and simplex schemes, is used to obtain the parameter set which minimized the least square error between predicted and actual data. Parameter sensitivity studies are conducted for the models examined. The ability to constrain parameters to a range of values is a means for allowing for the "fuzziness" of experimental data and model representations thereof. The use of computational optimization methods has proven effective; for example, the constants of the MTS model are similar to those reported in the literature for OFHC Cu. The determination of parameters for each of these models based on constant strain rate data is achieved rapidly with the numerical scheme compared to a manual procedure conducted by an expert user. These optimization procedures could be expanded in scope to develop improved functional forms for material representation in models, possibly in conjunction with artificial intelligence and pattern recognition algorithms that can discern and embed history effects.

It would also be a worthy objective to pursue a systematic study of ISV models with successively increasing numbers of state variables but with the same form of strain hardening for each.

Acknowledgements

The support of the US Army Research Office (Dr. K. Iyer, monitor) is gratefully acknowledged.

References

Bammann, D., 1990. Modeling the temperature and strain rate dependent large deformation of metals. Appl. Mech. Rev. 43, S312.

Bammann, D., Chiesa, M.L., Johnson, G.C., 1990a. A strain rate dependent flow surface model of plasticity. Sandia National Laboratory Report, SAND90-8227, Livermore, CA.

Bammann, D., Chiesa, M.L., McDonald, A., Kawahara, W.A., Dike, J.J., 1990b. Prediction of ductile failure in metal structures. In: Failure Criteria and Analysis in Dynamic Response, ASME, Metals Park, OH, 7.

Belavendram, N., 1995. Quality by Design. Prentice Hall, New York.

Chaboche, J.-L., 1989. Constitutive equations for cyclic plasticity and cyclic viscoplasticity. Int. J. Plasticity 5, 247.

Braasch, H., Estrin, Y., 1993. Parameter identification for a two-internal-variable constitutive model using the evolution strategy. In: Bertram, L.A., Brown, S.B., Freed, A.D. (Eds.), Material Parameter Estimation for Modern Constitutive Equations, vol. 43. ASME, New York, p. 47.

Cuitino, A.M., Ortiz, M., 1992. Computational modeling of single crystals. Modelling Simul. Mater. Sci. Eng. 1, 225.

Dave, V.R., Brown, S.B., 1994. Critical experiments used to determine flow relations for rate-dependent metal deformation. Int. J. Plasticity 10, 237.

Estrin, Y., 1991. A versatile unified constitutive model based on dislocation density evolution. In: Freed, A. D., Walker, K. P (Eds.), High Temperature Constitutive Modeling-Theory and Applications, vol. 26. ASME, New York, p. 65.

Follansbee, P.S., Kocks, U.F., 1988. A constitutive description of the deformation of copper based on the use of the mechanical threshold as an internal state variable. Acta Metall. 36, 81.

Gourdin, W.H., Lassila, D.H., 1991. Flow stress of OFE copper at strain rates from 10^{-3} to $10^{4}\,s^{-1}$: grain size effects and comparison to the mechanical threshold stress model. Acta. Metall. 39, 2337.

Graham, S., 1995. The stress state dependence of finite inelastic deformation behavior of FCC polycrystalline materials. M.S. thesis, Georgia Institute of Technology, GA.

Hart, E.W., 1976. Constitutive relations for the nonelastic deformation of metals. J. Engng. Mat. Tech. 15, 193.

Hibbitt, Karlsson, Sorensen, 1997. ABAQUS, V5. 6. Hibbitt, Karlsson and Sorensen, Inc. Pawtucket, RI.

Johnson, G.R., 1988. Implementation of simplified constitutive models in large computer codes. In: Rajendran, A.M., Nicholas, T. (Eds.), Dynamic Constitutive/Failure Models. AFWAL-TR-88-4229. Wright–Patterson AFB, OH. p. 409.

Jackson, K., Watts, M., Chen, X., Centala, P. Wang, X., Khan, A., 1997. Evolution of isotropic and kinematic hardening during finite plastic deformation for OFHC copper and 6061-T0 aluminum. In: Khan, A.K. (Ed.), Physics and Mechanics of Finite Plastic & Viscoplastic Deformation.

Johnson, G.R., Cook, W.H., 1983. A constitutive model and data for metals subjected to large strains, high strain rates and high temperatures. Proceedings of Seventh International Symposium on Ballistics, The Hague, The Netherlands, p. 541.

Johnson, G.R., Hoegfeldt, J.M., Lindholm, U.S., Nagy, A., 1983. Response of various metals to large torsional strains over a large range of strain rates—part 1: ductile metals. ASME J. Engng. Mat. Tech. 105, 42.

Klepaczko, J.R., Chiem, C.Y., 1986. On the sensitivity of f. c. c. metals, instantaneous rate sensitivity and rate sensitivity of strain Hardening. J. Mech. Phys. Solids 34, 29.

Klepaczko, J.R., 1988. Discussion of microstructural effects and their modeling at high rates of strain. Institute of Physics Conference Series 102, 283.

Kocks, U.F., Argon, A.S., Ashby, M.F., 1975. Thermodynamics and Kinetics of Slip. Prog. Mater. Sci., Vol. 19. Pergamon Press, New York.

Lathrop, J.F., 1996. BFIT—a program to analyze and fit the BCJ model parameters to experimental data. Sandia National Laboratory Report, SAND97-8218, Livermore, CA.

Lindholm, U.S., Chan, K.S., Thacker, B.H., 1993. On determining material constants for unified thermo-visco-plastic constitutive equations. In: Bertram, L.A., Brown, S.B., Freed, A.D. (Eds.), Material Parameter Estimation for Modern Constitutive Equations, vol. 43. ASME, New York, p. 183.

Lowe and Miller, 1986.

Maudlin, P.J., Wright, S.I., Gray III, G.T., House, J.W., 1995. Application of faceted yield surfaces for simulating compression tests of textured materials. In: Murr, L.E., Staudhammer, K.P., Meyers, M.A. (Eds.), Metallurgical and Materials Applications of Shock-Wave and High-Strain-Rate Phenomena. Elsevier Science, The Netherlands, p. 877.

McQueen, H.J., Jonas, J.J., 1975. Recovery and recrystallization during high temperature deformation. In: Arsenault, R.J. (Ed.), Treatise on Materials Science and Technology, vol. 6. Academic Press, New York, p. 393.

McDowell, D.L., 1992. A nonlinear kinematic hardening theory for cyclic thermoplasticity and thermoviscoplasticity. Int. J. Plasticity 8, 695.

Mecking, H., Kocks, U.F., 1981. Kinetics of flow and strain-hardening. Acta Metall. 29, 1865.

Meyers, M.A., 1994. Dynamic Behavior of Materials. Wiley, New York.

Muller, D., Hartmann, G., 1989. Identification of materials parameters for inelastic constitutive models using principles of biologic evolution. ASME J. Engng. Mater. Techn. 111, 299.

Pierre, D.A., 1969. Optimization Theory with Applications. Wiley, New York.

Prager, W., 1955. The theory of plasticity: a survey of recent achievements. Proc. Inst. Mech. Eng. 169, 41.

Sample, V.M., Jaworsli, A.P., Field, D.P., 1993. A comparison of parameter evaluation procedures for a two-internal state variable constitutive model. In: Bertram, L.A., Brown, S.B., Freed, A.D. (Eds.), Material Parameter Estimation for Modern Constitutive Equations, vol. 43. ASME, New York, p. 227.

Senseny, P.E., Fossum, A.F., 1993. Parameter evaluation for a viscoplastic constitutive model. In: Bertram, L.A., Brown, S.B., Freed, A.D. (Eds.), Material Parameter Estimation for Modern Constitutive Equations, vol. 43. ASME, New York, p. 243.

Tanner, A.B., 1998. Modeling temperature and strain rate history effects in OFHC Cu. Ph. D. thesis, Georgia Institute of Technology, GA.

Taylor, G.I., 1938. Plastic strain in metals. J. Inst. Metals 62, 307.

Van der Velden, A., Kokan, D., Culbreth, M., Gee, J., Hadenfeld, M., 1996. Pointer Optimization Software 1. 2. Synaps Inc., Atlanta, GA.